Physics of the Solid State, Vol. 46, No. 7, 2004, pp. 1311–1319. Translated from Fizika Tverdogo Tela, Vol. 46, No. 7, 2004, pp. 1271–1279.

LATTICE DYNAMICS AND PHASE TRANSITIONS

Lattice Dynamics and Raman Scattering Spectrum of Elpasolite Rb_2KScF_6: Comparative Analysis

S. N. Krylova*, A. N. Vtyurin*, A. Bulou, A. S. Krylov*, and N. G. Zamkova***

** Kirensky Institute of Physics, Siberian Division, Russian Academy of Sciences, Akademgorodok, Krasnoyarsk, 660036 Russia*

e-mail: slanky@iph.krasn.ru

*** Universite du Maine, Le Mans, Cedex 9, 72085 France*

Received September 26, 2003

Abstract—Raman scattering spectra of elpasolite Rb_2KScF_6 are studied in a wide temperature range including two phase transitions: from the cubic to the tetragonal phase and then to the monoclinic phase. The experimental Raman scattering spectrum is compared with the lattice vibration spectra of these phases calculated using an *ab initio* approach. A number of anomalies (caused by structural rearrangement during the phase transitions) are revealed and quantitatively analyzed in the ranges of both the intramolecular vibrations of the octahedron molecular ScF_6 ions and low-frequency intermolecular lattice vibrations. The interaction between low-frequency intramolecular vibrations and the intermolecular modes is found to be significant, and strong resonance interaction of the rotational soft modes (which are recovered below the phase transition points) with hard low-frequency vibrations of the rubidium ion sublattice is detected. These interactions are shown to substantially complicate the spectra. © *2004 MAIK "Nauka/Interperiodica".*

1. INTRODUCTION

The perovskite-like Rb_2KScF_6 crystal belongs to the family of $A_2B^{(1)}B^{(2)}X_6$ elpasolites, where A and B are metal cations or more complex molecular ions and X are oxygen or halogen anions [1]. As a rule, one of the highly polarized cations enters into the rather rigid octahedral molecular group BX_6 and the crystal structure can be considered a skeleton of these octahedra separated by cations with a strongly localized electron density. In many cases, phase transitions in elpasolites are related to changes in the octahedral skeleton, namely, small tilts of these octahedra or their orientation ordering. In particular, these changes manifest themselves experimentally in substantial anomalies in the crystal lattice dynamics, including the condensation of soft phonon modes during displacive transitions [1–5].

The Rb_2KScF_6 crystal undergoes phase transitions from the cubic to the tetragonal phase and then to the monoclinic phase [6]. The stability of these structures and the dynamics of their lattices were analyzed in [7, 8] by performing nonempirical calculations. It was shown that the instability of these structures is of phonon nature and that the mechanism of at least the first transition is related to the condensation of an optical phonon, which should appear again in the low-symmetry phases. Earlier searches for manifestations of such vibrations in Raman scattering spectra did not meet with success [9] (as in the cases of other fluorine-containing elpasolites [10]). Later, observation of the recovery of soft phonon modes in the Rb_2KScF_6 crystal was reported in [11, 12]. However, the number of these modes is inconsistent with that predicted by group-theoretic analysis [13] and they can be observed experimentally only well below the phase transition point. Therefore, the purpose of this work is to analyze the experimental spectral data quantitatively, compare them with the results of numerical calculations, and establish the causes of discrepancies between the calculated and experimental data.

2. CRYSTAL STRUCTURE AND SYMMETRY

The unit cell of the high-symmetry cubic phase of the elpasolite $A_2BB^{3+}X_6$ can be represented as a cubic perovskite cell with doubled parameters in which the B and B^{3+} ions alternate along all three coordinate axes. The structure of the unit cell (space group $Fm3m$, $Z = 4$) is shown in Fig. 1.

As the temperature decreases, the Rb_2KScF_6 crystal undergoes two sequential phase transitions: from the cubic to the tetragonal phase (space group $I114/m$, $Z = 2$) at $T_1 = 252$ K and then to the monoclinic phase (space group $P12_1/n1$, $Z = 2$) at $T_2 = 223$ K [6]. The calculated distortion of the structure [8] that is predicted to occur at the first phase transition is shown in Fig. 2. As is seen, this distortion is a rotation of the rigid ScF_6 octahedra.

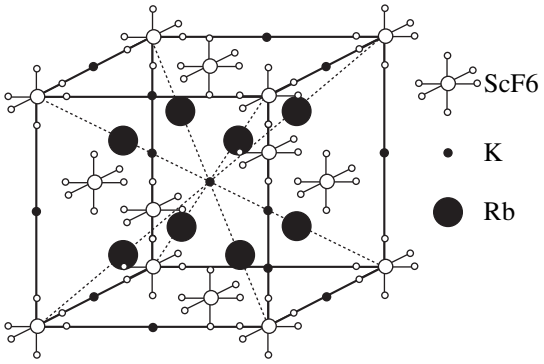

Fig. 1. Structure of the initial cubic phase of the Rb_2KScF_6 crystal.

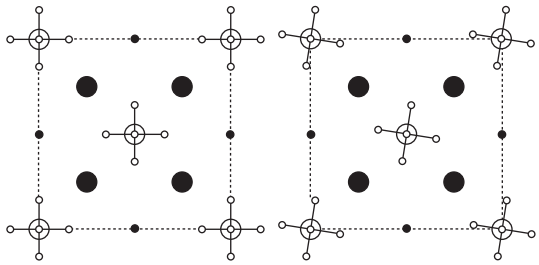

Fig. 2. Lattice distortions associated with the transition to the tetragonal phase.

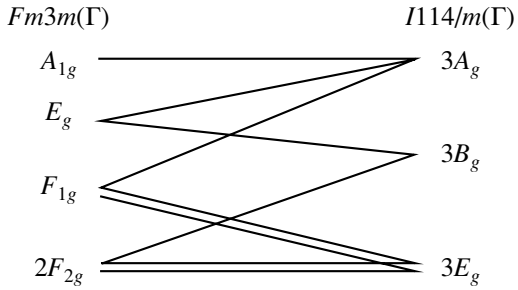

Fig. 3. Correlation diagrams for the Raman-active vibrations of the cubic and tetragonal phases.

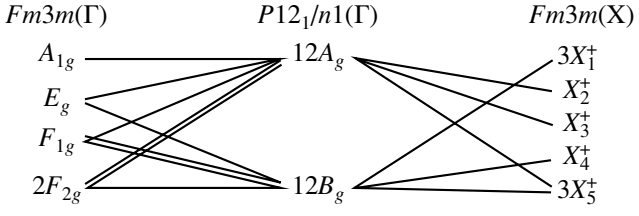

Fig. 4. Correlation diagrams for the Raman-active vibrations of the cubic and monoclinic phases.

In the high-symmetry cubic phase, the reduction of the oscillation representation at the center of the Brillouin zone is

$$\Gamma_{\text{vibr}}(Fm3m) = A_{1g}(xx, yy, zz) + E_g(xx, yy, zz) + 2F_{2g}(xz, yz, xy) + F_{1g} + 5F_{1u} + F_{2u}. \quad (1)$$

The Raman tensor components in which the corresponding vibrations are active are indicated in parentheses. The intramolecular modes related to the internal vibrational degrees of freedom in the ScF_6 octahedron in the crystal can be considered to interact only weakly with intermolecular lattice vibrations related to the rigid motion of the octahedron as a whole and to remain strongly localized, which agrees with the data from [10–13]. In this case, in the cubic phase, only the intermolecular mode F_{2g} is Raman-active; the other Raman-active modes are the intramolecular vibrations of this group.

Since the symmetry of the free octahedron coincides with the symmetry of the position of the ScF_6 groups in the crystal, the symmetry and shape of their intramolecular vibrations should remain unchanged in this approximation [14].

In the tetragonal phase, the reduction of the oscillation representation at the center of the Brillouin zone has the form

$$\Gamma_{\text{vibr}}(I114/m) = 3A_g(xx, yy, zz) + 3B_g(xx, yy, xy) + 3E_g(xz, yz) + 5A_u + B_u + 6E_u. \quad (2)$$

Figure 3 shows the correlation diagram for vibrations (1) and (2).

The structural distortions due to the first phase transition (Fig. 2) transform according to the triply degenerate irreducible representation F_{1g}. Therefore, the soft mode above the transition point should also transform according to this representation; this mode is inactive in the Raman scattering spectra (and the infrared absorption spectra).

From the correlation diagram in Fig. 3, it follows that, below the transition point to the tetragonal phase, the degeneracy of the intramolecular (E_g, F_{2g}) and intermolecular (F_{2g}) vibrations can be removed (i.e., splitting will occur) and two soft modes can split and become Raman-active.

In the low-symmetry monoclinic phase, the reduction of the oscillation representation of the symmetry group has the form

$$\Gamma_{\text{vibr}}(P12_1/n1) = 12A_g(xx, yy, zz, xy, yx) + 12B_g(xz, yz, zx, zy) + 18A_u + 18B_u. \quad (3)$$

The transition to the monoclinic phase is accompanied by a twofold increase in the unit cell volume. The modes at the $X(0, 0, \pi/a)$ point in the Brillouin zone, including the possible soft mode X_2^+, are Raman-inactive; however, they can become Raman-active below

the second transition point (and the soft mode can also be recovered). The correlation between the Raman-active modes in the monoclinic phase and the modes in the cubic phase is shown in Fig. 4. As is seen, the mode X_2^+ is the only one in this structure and it corresponds to rotation of the octahedral groups. We might also expect further splitting of the modes that are degenerate in the tetragonal phase, including the recovering soft mode corresponding to the transition from the cubic to the tetragonal phase.

3. EXPERIMENTAL AND DATA PROCESSING TECHNIQUES

To study Raman spectra, we applied polarized 514.5-nm radiation from a 500-mW Ar^+ laser as an excitation source. The spectra were recorded in the 180° geometry using a T-64000 spectrometer (I.S.A., Jobin Yvon) with matrix recording. Samples $2 \times 2 \times 4$ mm in size were taken from the solidification batch used in [6, 11]; their edges were orientated along the crystallographic axes of the cubic phase. The samples are optically transparent and do not contain color defects or inclusions that are visible under a microscope. To weaken the wing of elastic scattering as much as possible to record low-frequency spectra, we applied a triple monochromator in the dispersion subtraction mode. Low frequencies were cut beginning from 8 cm^{-1}. To record high-resolution spectra of intramolecular vibrations (with minimum distortion of line contours), we applied the dispersion addition mode. The spectral size of the recording matrix cell was 650/1024 cm^{-1} in the dispersion subtraction mode and 220/1024 cm^{-1} in the dispersion addition mode; the counting time was 600 s. The temperature of a sample during the recording of spectra was maintained with an accuracy of better than 0.2 K. The Rb_2KScF_6 crystal was studied in the temperature range 50–600 K.

To determine the parameters of spectral lines, we processed the experimental data with the SigmaPlot 8.0 software package using the dispersion shape of a contour. Moreover, we took into account the frequency-dependent correction

$$I_s(\Omega_\alpha) \sim |Q_\alpha|^2 \sim n_\alpha + 1 = \frac{1}{1 - \exp(-\hbar\Omega_\alpha/k_B T)} \quad (4)$$

to the temperature dependence of the scattering intensity.

To correctly compare the experimental Raman spectra with the calculations carried out in [7, 8] and determine the eigenvectors of the observed vibrations, we performed a group-theoretic analysis of the eigenvectors of the calculated lattice vibrations. For this purpose, the calculated eigenvectors of the dynamic matrix are expanded in terms of the basis functions of the irreducible representations of the crystal symmetry group using projection operators. We constructed the complete oscillation representation $P(g)$ of the space group of the hexagonal phase and then found the projection operators [15]:

$$P_\rho = \frac{d(\rho)}{N(g)} \sum_{g \in G} \chi_\rho(g) P(g). \quad (5)$$

Here, $d(\rho)$ is the dimension of the representation ρ of the point symmetry operation, $N(g)$ is the dimension of the symmetry group, $\chi_\rho(g)$ is the character of the matrix of the irreducible representation ρ, $P(g)$ is the oscillation representation of the symmetry operation for the irreducible representation ρ of the group G, and P_ρ is the projection operator. Summation is performed over all operations of the symmetry group. A vibration eigenvector **f** is transformed according to the irreducible representation ρ of the group G if it satisfies the criterion [15]

$$P_\rho \mathbf{f} = \frac{N(g)}{d(\rho)} \mathbf{f}. \quad (6)$$

This algorithm of expansion of the eigenvectors of a dynamic matrix in terms of the irreducible representations is realized using the Mathematica 4.2 software package.

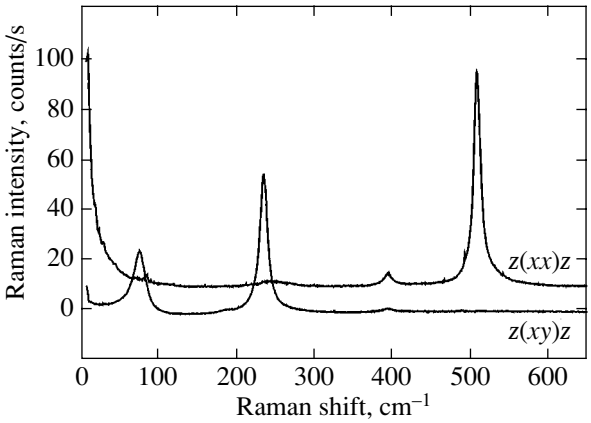

Fig. 5. Raman spectrum of the cubic phase of Rb_2KScF_6 (T = 300 K).

4. EXPERIMENTAL RESULTS AND DISCUSSION

4.1. Raman Scattering Spectrum of the Cubic Phase

The spectrum of the Rb_2KScF_6 cubic crystal far from the phase transition point is shown in Fig. 5. In Table 1, the calculated modes of the cubic phase [7] are assigned to the symmetry types and the experimental frequencies are compared with the corresponding calculated frequencies.

The number, frequencies, and polarization of the spectral lines of the cubic phase agree well with those observed earlier [9–13]. The lines are strongly polar-

Table 1. Experimental and calculated vibration frequencies (cm^{-1}) of Rb_2KScF_6 in the cubic phase

Vibration mode	Calculation [7]	Experiment
F_{1g}	**66i**	
F_{1u}	34i	
F_{2g}	26i	89
F_{1u}	0	
F_{1u}	80	
F_{2u}	99	
F_{1u}	135	
F_{2g}	152	230
F_{1u}	164	
F_{1u}	185	
F_{1u}	189	
E_g	343	390
A_{1g}	402	505
F_{1u}	404	
F_{1u}	462	

Note: Boldface type shows the calculated frequency of the soft mode corresponding to the first phase transition.

ized, which confirms the high quality of the sample. The calculated frequencies are somewhat lower than the experimental ones, which can be due to the fact that the calculations correspond to the absolute zero of temperature, where the cubic phase is unstable. This circumstance also explains the imaginary values of the frequencies of the low-frequency vibrations.

Table 2 gives examples for the eigenvectors of intramolecular vibrations of the ScF_6 octahedra. As was expected, the eigenvectors of the two highest frequency vibration modes (390 and 505 cm^{-1}) correspond to intramolecular vibrations of the free ScF_6 octahedra (390 and 498 cm^{-1} for the free ScF_6 ion, respectively [14]). However, the low-frequency intramolecular vibration of the octahedral ion and the intermolecular vibration mode of the rubidium ion sublattice (both vibrations have the F_{2g} symmetry) are found to be mixed, although their vibration frequencies are rather far from each other (230 and 89 cm^{-1}, respectively). This finding indicates noticeable interaction between the intermolecular and the intramolecular vibrations even in the high-symmetry cubic phase.

4.2. Temperature Dependence of the Internal Vibration Modes

The correlation diagrams of the Raman-active internal modes are given in Fig. 6. It is seen that, below the transition to the monoclinic phase, an additional line corresponding to the Brillouin zone boundary can appear in the region of the fully symmetrical high-frequency vibration of the ScF_6 group.

The transformation of the spectrum in the frequency range in question is shown in Fig. 7, and the temperature dependences of the frequencies and half-widths of the observed lines are shown in Fig. 8. In Fig. 7, additional lines are clearly seen to appear in this spectral region at low temperatures, which agrees well with the selection rules (see the correlation diagram in Fig. 6). The temperature dependence of the frequency significantly changes in character near the phase transformation points. Extrapolating the temperature dependence of the frequency in the cubic phase using the well-known relation [12, 13] (see Fig. 8)

$$\Omega_\alpha(T) = \Omega_\alpha(0)\exp(-3\gamma_\alpha\alpha T) \qquad (7)$$

gives the product of the Grüneisen parameter by the coefficient of thermal expansion, $\gamma_\alpha\alpha \approx 0.2 \times 10^{-5}$ K^{-1}. The frequency extrapolated to zero temperature is equal to 518 cm^{-1}. Such a low value of the Grüneisen param-

Table 2. Eigenvectors of the internal vibrations of the ScF_6 ion

	E_g						A_{1g}		
Atom	*x*	*y*	*z*	*x*	*y*	*z*	*x*	*y*	*z*
Rb	0	0	0	0	0	0	0	0	0
Rb	0	0	0	0	0	0	0	0	0
K	0	0	0	0	0	0	0	0	0
Sc	0	0	0	0	0	0	0	0	0
F	0	0	0.29	0	0	0.5	0	0	−0.41
F	0	0	−0.29	0	0	−0.5	0	0	0.41
F	0.29	0	0	0.5	0	0	0.41	0	0
F	−0.29	0	0	−0.5	0	0	−0.41	0	0
F	0	−0.58	0	0	0	0	0	−0.41	0
F	0	0.58	0	0	0	0	0	0.41	0

eter, even making allowance for its dependence on the frequency

$$\gamma_\alpha = \frac{B_T}{\Omega_\alpha}\left(\frac{d\Omega_\alpha}{dP}\right)_T \quad (8)$$

indicates that the effect of anharmonicity on this vibration is weak (Ω_α is the frequency of this vibration, B_T is the isothermal bulk modulus of elasticity, P is the hydrostatic pressure).

The frequency shift with respect to the extrapolated value below the transition to the tetragonal phase is shown in Fig. 9.

A small additional frequency shift appears even in the cubic phase in a rather wide (about 50 K) region above the phase transition point. The shift increases monotonically in the tetragonal phase and becomes virtually linear in the monoclinic phase, which corresponds to a second-order (or close-to-second-order) phase transformation.

The half-width of this line also changes with temperature. Its temperature dependence is shown in Fig. 10. The curve in Fig. 10 is the half-width in the cubic phase fitted by the expression

$$\sigma(\Omega_\alpha, T) = \sigma(\Omega_\alpha, 0)\left(1 + \frac{1}{\exp(\hbar\Omega_{\beta1}/k_B T) - 1} + \frac{1}{\exp(\hbar\Omega_{\beta2}/k_B T) - 1}\right) \quad (9)$$

which describes the line broadening caused by the decay into two phonons [16, 17]. The experimental dependence is seen to be correctly described by this expression; this fact indicates the absence of substantial contributions from other line-broadening mechanisms, e.g., structural disordering of the crystal in the high-temperature phase. The fitted frequencies of the phonons involved in the decay of this intramolecular vibration are found to be $\Omega_{\beta1} \approx 413$ cm^{-1} and $\Omega_{\beta_2} = \Omega_\alpha - \Omega_{\beta1}$, which correspond to a decay into two optical phonons with one of the phonons being close in frequency to the intramolecular vibration ν_2 [14] and the other falling in the region of high-frequency lattice vibrations. The line half-width extrapolated to zero temperature is 0.9 cm^{-1}.

As follows from Fig. 5, the intramolecular vibration ν_2 in the cubic phase is very weak; for this reason, we failed to reliably detect its splitting below the phase transition points. The temperature dependence of its frequency is also described well by Eq. (7) with $\gamma_\alpha\alpha \approx 0.4 \times 10^{-4}$ K^{-1}, which corresponds to a higher value of the Grüneisen parameter (i.e., greater anharmonicity of vibrations); the frequency extrapolated to zero temperature is equal to 407 cm^{-1}.

The temperature dependences of the frequencies and half-widths of the lines detected in the region of the intramolecular vibration ν_5 are shown in Fig. 11. The

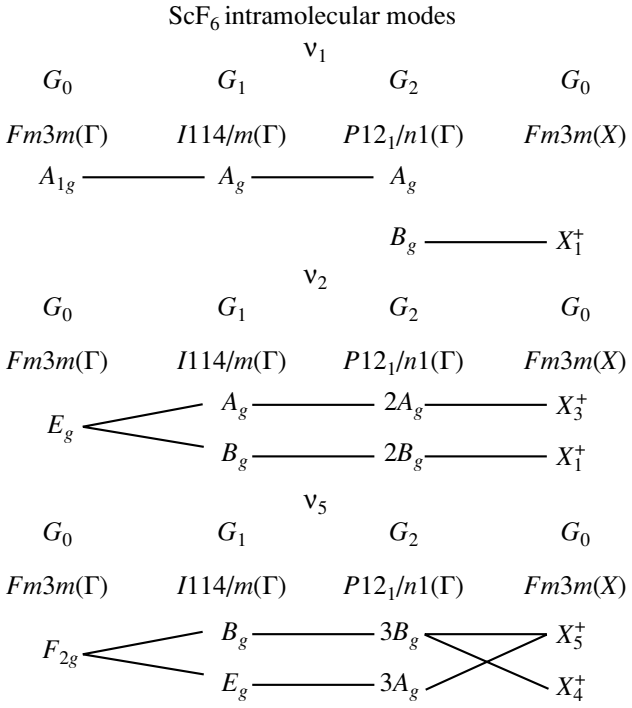

Fig. 6. Correlation diagrams for the Raman-active internal vibrations of the ScF_6 groups. The vibrations that are allowed in the spectrum by the selection rules are marked.

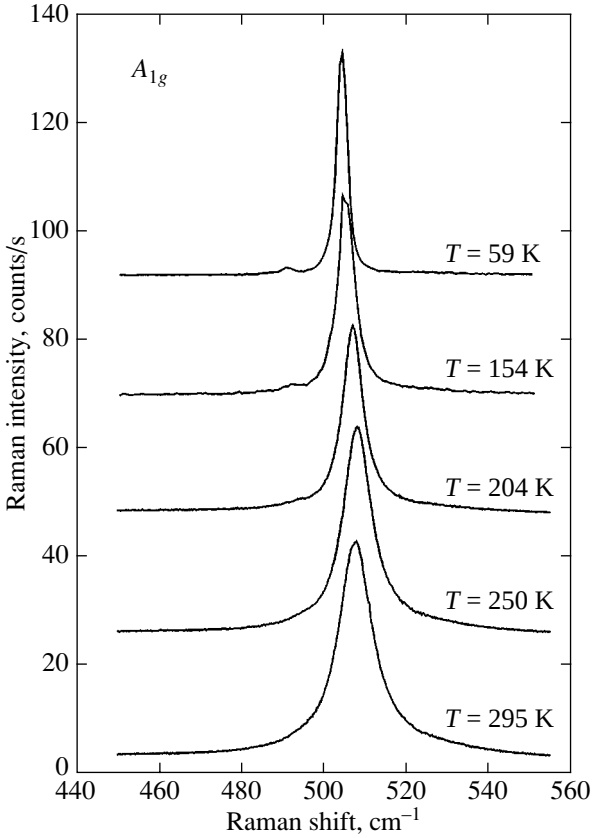

Fig. 7. Variation of the Raman spectrum in the region of the fully symmetrical internal vibration with temperature.

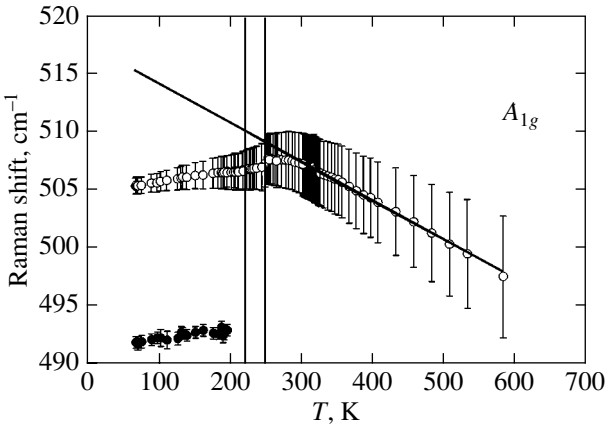

Fig. 8. Temperature dependences of the frequencies of the lines corresponding to the fully symmetrical internal vibration. The vertical bars show their half-widths at half-maximum (HWHM).

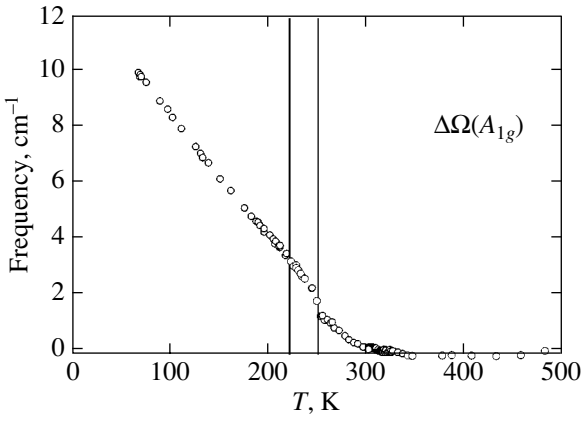

Fig. 9. Temperature dependence of the frequency shift of the fully symmetrical internal vibration with respect to the extrapolated value.

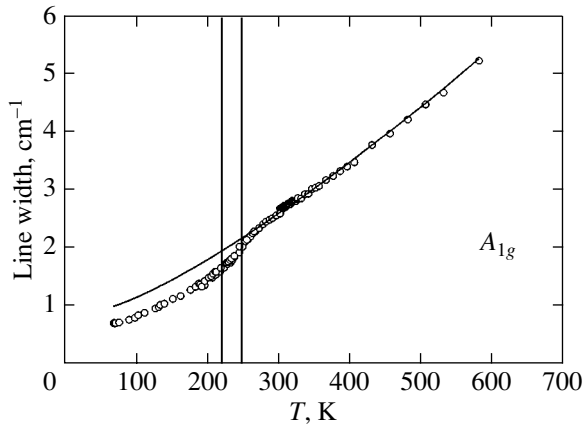

Fig. 10. Temperature dependence of the half-width at half-maximum (HWHM) of the internal vibration ν_1. The curve is extrapolation by Eq. (9).

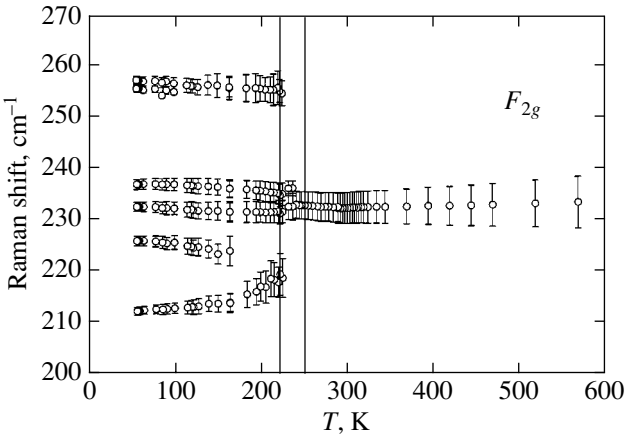

Fig. 11. Temperature dependences of the line frequencies in the region of the internal vibration ν_5. The vertical bars show the line half-widths (HWHM).

number of the lines corresponds to the selection rules (Fig. 6), and their positions agree qualitatively with the calculations [7].

The frequency of the most intense line in this range (232 cm^{-1}) remains virtually unchanged in the cubic phase, which indicates that the contributions from thermal expansion and phonon–phonon interaction to the temperature dependence of the frequency compensate each other. Below the transition from the cubic to the tetragonal phase, the frequency of this line changes continuously and the line splits to form a doublet. At the transition to the monoclinic phase, the frequencies change in a jump and split further. The continuous variation of the spectrum during the first phase transition and the jumpwise change during the second transition agree with the data on the thermodynamics of these transitions [6]. The lines that appear in the monoclinic phase and correspond to the Brillouin zone boundary of the cubic phase are very weak, and some of them can be detected only far below the transition to the monoclinic phase.

The temperature dependence of the half-width of the line at 232 cm^{-1} fitted by Eq. (9) gives a value of 0.1 cm^{-1} for the line half-width extrapolated to $T = 0$ and a frequency of 224 cm^{-1} for the phonon that forms during decay; this frequency corresponds to the decay into an optical and acoustic phonons at the Brillouin zone boundary.

4.3. Temperature Dependence of the Lattice Vibration Modes

The variation of the intermolecular vibration spectrum with temperature is shown in Fig. 12. The spec-

trum can be divided into two portions, above and below 60 cm^{-1}. The higher frequency spectrum corresponds to stable (hard) intermolecular vibration modes of the rubidium ion sublattice with a small admixture of the low-frequency intramolecular deformation vibration mode of the ScF_6 ions. (The eigenvector of this mode, as well as the eigenvector of the Raman-inactive soft mode in the cubic phase, is given in Table 3). In this range, the frequency of the intermolecular mode grows slowly (89 cm^{-1} at room temperature). Below the first transition point, this mode splits into two lines and then splits further below the second transition point and additional low-intensity lines appear upon deeper cooling. The temperature dependences of the frequencies and widths of these lines are shown in Fig. 13.

The total number of lines detected in this higher frequency range corresponds to the selection rules (see the correlation diagram in Fig. 14).

Note that new lines appear immediately after the phase transitions, which is related to the splitting of degenerate vibration modes in the high-symmetry phases. However, the additional lines caused by a twofold increase in the unit cell volume appear far below the phase transition points. This finding can be explained by the fact that the phase transitions result in substantial changes in the crystal dynamics, which leads to shifts and splitting of the lines corresponding to Raman-active modes in the high-temperature phase. At the same time, the derivatives of the crystal dielectric susceptibility with respect to the atomic displacements change only weakly and the forbidden vibrations at the Brillouin zone boundary remain weak until their eigenvectors become sufficiently strongly distorted.

In the low-frequency portion of the spectrum (<60 cm^{-1}), the central scattering peak grows and broadens as the temperature decreases in the region several degrees above the phase transition point. Below the first transition point, a wide wing (which can be interpreted as the excitation of a low-intensity broad band) appears near the central peak (Fig. 15). At lower temperatures, this band exhibits two maxima, at 26 and 39 cm^{-1}. Figure 15 shows the temperature dependence of the squared frequencies of the maxima of these lines.

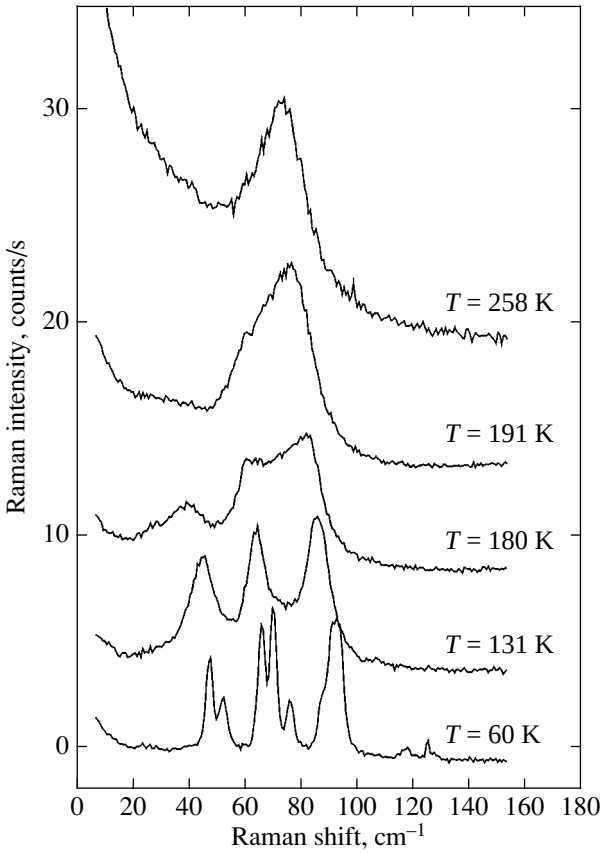

Fig. 12. Variation of the lattice vibration spectrum of Rb_2KScF_6 with temperature.

In the tetragonal phase, no significant shifts in the frequencies of these lines are observed (the accuracy of

Table 3. Eigenvectors of lattice vibration modes in the cubic phase

Hard F_{2g} mode, Ω = 89 cm^{-1}				Soft F_{1g} mode, $\Omega = 66i$ cm^{-1}		
Atom	x	y	z	x	y	z
Rb	0.35	−0.52	0.18	0	0	0
Rb	−0.35	0.52	−0.18	0	0	0
K	0	0	0	0	0	0
Sc	0	0	0	0	0	0
F	−0.16	0.10	0	0.39	0.08	0
F	0.16	−0.10	0	−0.39	−0.08	0
F	0	−0.05	0.16	0	0.31	0.39
F	0	0.05	−0.16	0	−0.31	−0.39
F	0.05	0	0.10	0.31	0	−0.08
F	−0.05	0	−0.10	−0.31	0	0.08

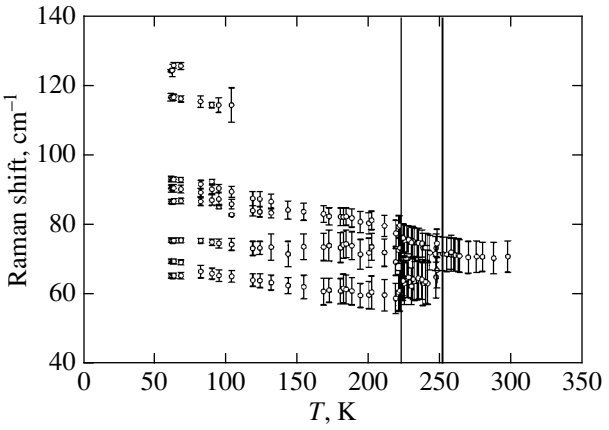

Fig. 13. Temperature dependences of the frequencies of the Rb_2KScF_6 hard lattice vibration modes. The vertical bars show the line half-widths (HWHM).

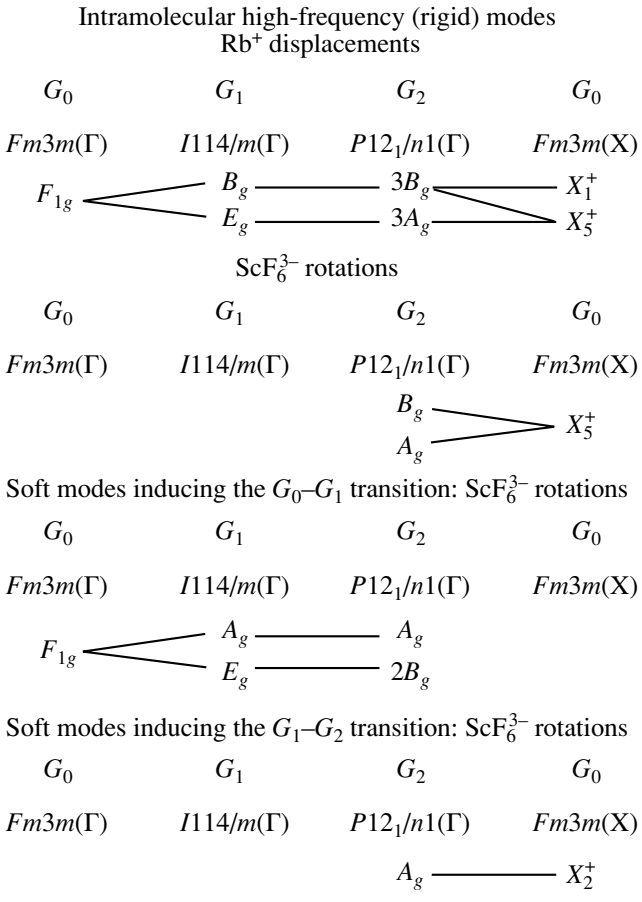

Fig. 14. Correlation diagrams for the Raman-active lattice vibrations. The vibrations that are allowed in the spectrum by the selection rules are marked.

determining the line positions is low, because the noise level is comparable to the line intensities). We note only a transfer of intensity to the high-frequency portion of this band and a decrease in the intensity of the central peak (which is likely due to rearrangement of the domain structure) with decreasing temperature.

When the second transition point is reached, the intensity of elastic scattering increases jumpwise and the intensity of the detected band is redistributed; namely, its high-frequency portion increases substantially. The frequency of this maximum increases monotonically upon cooling, and the temperature dependence of the frequency squared is almost linear, which is characteristic of the soft modes related to displacive second-order (or close-to-second-order) phase transitions. Below 100 K, where the lines become strongly narrower because of small anharmonicity at such temperatures, this maximum splits in two. As the temperature decreases further, the high-frequency component of the doublet formed continues to move upward, whereas the position of the low-frequency component remains virtually unchanged (47–48 cm^{-1}).

The position of the lowest frequency maximum also remains virtually unchanged (23–27 cm^{-1}). Its intensity decreases slowly, and, below 100 K, it can hardly be detected against the noise background.

The number of lines observed in the lattice vibration spectra is consistent with the selection rules (see the correlation diagram in Fig. 14). This diagram shows that, below the first transition point, the two modes will be observed that are formed as a result of the condensation and partial splitting of the earlier Raman-inactive F_{1g} phonon, which corresponds to rotational vibrations of the octahedron groups prior to the transition (Table 3). By analogy with the hard intermolecular modes, we might expect their intensities to be rather low. After the second phase transition, they should split to yield a triplet (the symmetry of the corresponding vibrations in the monoclinic phase is $A_g + 2B_g$). Simultaneously, the soft

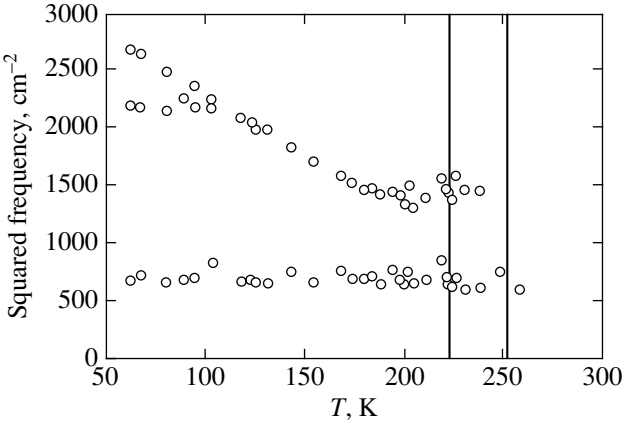

Fig. 15. Temperature dependence of the squared frequencies of the detected low-frequency lattice vibrations.

mode corresponding to this transition should begin to recover; this mode also has the A_g symmetry in the monoclinic phase and also corresponds to rotations of the octahedron groups in the high-temperature phase. The presence of the hard vibration modes of the rubidium ion sublattice of the same symmetry in the spectrum (Fig. 14; the calculated frequencies and eigenvectors of all lattice vibrations in the monoclinic phase can be found in [18]) leads to their resonance interaction with the recovering soft modes. This mode interaction is accompanied by strong mixing of their eigenvectors until the high-frequency component of the "soft multiplet" shifts toward sufficiently high frequencies, where it becomes observable in the experimental spectrum. Note that, according to the dynamics calculations of the monoclinic phase at $T = 0$ [7], the frequencies of the two lowest vibration modes in the spectrum are 22 and 31 cm^{-1}, which agrees well with the experimental position of the low-frequency maximum (23–27 cm^{-1}). However, calculations [18] show that the eigenvector of these vibrations is a superposition of the rotations of the rigid ScF_6 groups (without distortion) and the displacements of the rubidium atoms.

5. CONCLUSIONS

The phase transitions in Rb_2KScF_6 have been found to be accompanied by the recovery of soft phonon modes, which allows us to attribute them to displacive transitions [8, 9]. We did not detect any lattice disordering–induced anomalies in the lattice dynamics of the high-symmetry phase. The group-theoretic analysis shows that the eigenvectors of both soft modes above the phase transition points are connected with the rotations of the ScF_6^+ octahedron molecular ions. Below the transition to the monoclinic phase, a strong interaction between the recovering rotational soft modes and the displacements of the rubidium ions is observed. This interaction results in modification of the temperature dependences of the phonon frequencies and mixing of the phonon eigenvectors and complicates the vibration spectrum.

Anomalies in the temperature dependences of the parameters of the hard intermolecular modes and the intramolecular vibrations of the $KScF_6$ groups have been revealed and interpreted. Quantitative analysis of these anomalies supported the transition to the tetragonal phase being a second-order transition and the transition to the monoclinic phase being a first-order (close-to-second-order) transition. The small values of the line half-widths and their temperature dependences indicate that the vibration damping in the high-symmetry phase is determined by the decay of phonons due to their anharmonicity and is not related to structure disordering, except, possibly, for the pretransition region.

ACKNOWLEDGMENTS

The authors thank K.S. Aleksandrov, I.N. Flerov, and V.I. Zinenko for supplying the samples and for valuable discussions.

This work was supported jointly by the Russian Foundation for Basic Research and the Krasnoyarsk Science Foundation (project Eniseĭ, no. 02-02-97707) and the Siberian Division of the Russian Academy of Sciences (project no. 88).

REFERENCES

1. K. S. Aleksandrov and B. V. Beznosikov, *Perovskite-like Crystals* (Nauka, Novosibirsk, 1997).
2. W. Buhrer and H. U. Gudel, J. Phys. C **20**, 3809 (1987).
3. G. P. Knudsen, Solid State Commun. **49**, 1045 (1984).
4. F. Prokert and K. S. Aleksandrov, Phys. Status Solidi B **124**, 503 (1984).
5. G. Baldinozzi, Ph. Sciau, and A. J. Bulou, J. Phys.: Condens. Matter **7**, 8109 (1995).
6. I. N. Flerov, M. V. Gorev, S. V. Mel'nikova, S. V. Misyul', V. N. Voronov, and K. S. Aleksandrov, Fiz. Tverd. Tela (St. Petersburg) **34**, 2185 (1992) [Sov. Phys. Solid State **34**, 1168 (1992)].
7. V. I. Zinenko and N. G. Zamkova, Fiz. Tverd. Tela (St. Petersburg) **41**, 1297 (1999) [Phys. Solid State **41**, 1185 (1999)].
8. V. I. Zinenko and N. G. Zamkova, Zh. Éksp. Teor. Fiz. **118**, 359 (2000) [JETP **91**, 314 (2000)].
9. I. N. Flerov, M. V. Gorev, K. S. Aleksandrov, A. Tressaud, J. Grannec, and M. Cousi, Mater. Sci. Eng. R **24**, 81 (1998).
10. M. Cousi, S. Khairoun, and A. Tressaud, Phys. Status Solidi A **98**, 423 (1986).
11. A. N. Vtyurin, A. Bulou, A. S. Krylov, and V. N. Voronov, Fiz. Tverd. Tela (St. Petersburg) **43**, 2066 (2001) [Phys. Solid State **43**, 2154 (2001)].
12. A. S. Krylov, A. N. Vtyurin, A. Bulou, and V. N. Voronov, Ferroelectrics **284**, 47 (2003).
13. A. N. Vtyurin, A. Bulou, A. S. Krylov, and V. N. Voronov, Preprint No. 815F, IF SO RAN (Inst. of Physics, Siberian Division, Russian Academy of Sciences, Krasnoyarsk, 2002).
14. K. Nakamoto, *Infrared and Raman Spectra of Inorganic and Coordination Compounds* (Wiley, New York, 1986; Mir, Moscow, 1991).
15. H. Streitwolf, *Gruppentheorie in der Festkörperphysik* (Teubner, Leipzig, 1967; Mir, Moscow, 1971).
16. M. Balkanski, R. F. Wallis, and E. Haro, Phys. Rev. B **28**, 1928 (1983).
17. J. Gonzalez, E. Moya, and J. C. Chervin, Phys. Rev. B **54**, 4707 (1996).
18. S. N. Krylova, A. N. Vtyurin, A. Bulou, A. S. Krylov, and N. G. Zamkova, Preprint No. 821F, IF SO RAN (Inst. of Physics, Siberian Division, Russian Academy of Sciences, Krasnoyarsk, 2003).

Translated by K. Shakhlevich